Quasiparticle lifetime broadening in resonant x-ray scattering of NH_4NO_3

John Vinson and Terrence Jach
Material Measurement Laboratory, National Institute of Standards and Technology, Gaithersburg, Maryland 20899, USA

Matthias Müller, Rainer Unterumsberger, and Burkhard Beckhoff
Physikalisch-Technische Bundesanstalt, Abbestraße 2-12, 10587 Berlin, Germany
(Received 13 January 2016; revised manuscript received 15 April 2016; published 29 July 2016)

It has been previously shown that two effects cause dramatic changes in the x-ray absorption and emission spectra from the N K edge of the insulating crystal ammonium nitrate. First, vibrational disorder causes major changes in the absorption spectrum, originating not only from the thermal population of phonons, but, significantly, from zero-point motion as well. Second, the anomalously large broadening ($\sim$4 eV) of the emission originating from nitrate σ states is due to the unusually short lifetimes of quasiparticles in an otherwise extremely narrow band. In this work, we investigate the coupling of these effects to core and valence excitons that are created as the initial x-ray excitation energy is progressively reduced toward the N edge. Using a GW/Bethe-Salpeter approach, we show the extent to which this anomalous broadening is captured by the GW approximation. The data and calculations demonstrate the importance that the complex self-energies (finite lifetimes) of the valence bands have on the interpretation of emission spectra. We produce a scheme to explain why extreme lifetimes should appear in σ states of other similar compounds.

DOI: 10.1103/PhysRevB.94.035163

I. INTRODUCTION

We recently presented a comparison of theory and experiment, looking at the x-ray absorption and emission from (to) the nitrogen 1s in several ionic crystals [1]. Line broadening and suppression effects observed in x-ray absorption spectra (XAS) from the compounds NH_4Cl and NH_4NO_3 were attributed to phonon disorder in the lattice, and the zero-point motion of high-frequency 1000 to 3000 cm^{-1} phonon modes proved to be significant ($k_BT \approx 200$ cm^{-1} at room temperature). The inclusion of these effects brings the calculated absorption into a considerable degree of agreement with the observed XAS. The emission spectra from both compounds showed evidence of atomic disorder as well, but also an unexpected extreme broadening ($\sim$4 eV) of one of the emission lines of NH_4NO_3. This anomalous broadening was explained by a many-body effect that causes strong lifetime broadening in the quasiparticles associated with the NO σ bonds.

The results described previously were only evaluated for x-ray emission spectra (XES) at incident energies well above the K edge of nitrogen. The situation becomes even more complex as the energy decreases towards the vicinity of an excitation edge. Referred to as resonant inelastic x-ray scattering (RIXS), x-ray emission has a strong sensitivity to the initial excitation energy in the region at and just above the absorption edge. As a lowest-order approximation this can be thought of as a convolution of occupied and unoccupied densities of states as probed by the core excitations, but strong electron-hole interactions near the threshold can result in complex excitonic behavior [2]. Nevertheless, a calculation of emission spectra using the Bethe-Salpeter equation, evaluated for an ensemble of snapshots of lattice disorder, provides a remarkably accurate description of changes in the XES.

With two inequivalent N sites on the NH_4^+ cation and NO_3^- anion, ammonium nitrate is a well-suited model system for evaluating various contributions to x-ray spectra. In this paper, we demonstrate the effects of vibrational disorder and lifetime broadening in a comparison with measurements of RIXS of NH_4NO_3 at excitation energies progressively decreasing from 25 eV above the nitrogen K edge. We show the origins of, and have developed a criterion for, the presence of the anomalous broadening in XES.

II. EXPERIMENTAL SETUP

The experiments were carried out at the plane grating monochromator (PGM) beamline for undulator radiation in the PTB laboratory at the electron storage ring BESSY II [3,4]. The beamline provides tunable radiation in the soft x-ray range with high spectral purity and photon flux. The undulator radiation is focused on the sample and the fluorescence radiation is detected using a spherical grating spectrometer on a Rowland circle with a CCD detector [5,6]. The monochromator was calibrated by measuring the N K-absorption spectrum of N_2 gas in a cell as detected by a photodiode. Multiple vibrational bands were fitted assuming the value for the first vibrational peak corresponding to the initial $1s$-$1\pi_g^*$ band transition of 400.70 eV [7]. The standard uncertainty of the monochromator fit to the vibrational peaks was 105 meV. The photodiode was also used to normalize the photon flux over the energy range of the scan.

The emission spectrometer consisted of a spherical grating with a pitch of 1200 lines/mm on a Rowland circle of 2.5 m radius with a CCD detector of 1024 channels along the dispersive direction and 1024 transverse channels in the grating plane. The emission spectrometer was calibrated using elastic scattering of the monochromatic radiation from a BN sample over a range of 15 eV. The uncertainty of the spectrometer calibration was 60 meV, giving a combined uncertainty of 121 meV. The acceptance of the CCD gave a range of 40 eV, and therefore at each excitation energy the entire XES was recorded simultaneously.

The samples consisted of ammonium nitrate microcrystalline powder (99.89% purity) that was pressed into an indium foil and mounted in high vacuum. All measurements were carried out at room temperature. Absorption spectra were obtained by monitoring the N Kα line fluorescence intensity with a Si drift detector (SDD). The fluorescence intensities need to be corrected for self-absorption in order to have a true x-ray absorption spectrum (XAS). This was done by using a previously obtained, experimental ratio for the same compound of electron escape (short mean free path) versus total fluorescence (long mean free path) as a function of energy. The radiation damage to the sample was minimized by measuring each XES over multiple points on the sample and combining the results. XES were accumulated at each excitation energy for 4200 s.

III. COMPUTATIONAL APPROACH

We calculate our spectra using OCEAN [8,9], which builds on single-particle electron wave functions of the system from either density functional theory (DFT) or many-body GW calculations as outlined in Sec. III A. The OCEAN package relies on external codes for both the DFT and GW calculations. Details of OCEAN are provided in Sec. III B, and the treatment of disorder and vibrations is covered in Sec. III C.

A. Electronic ground state and self-energy effects

Density functional theory (DFT) is a widely used method for determining electronic ground-state properties of condensed matter systems. In DFT, the many-body interaction terms in the Hamiltonian are replaced with an energy functional of the density, reducing the computational cost significantly. The success and popularity of DFT is owed to the utility of the eigenstates, or Kohn-Sham orbitals, in calculations of ground-state properties: phase stability, conductance, etc. Formally, only the density of the DFT system will match the interacting system, and the DFT orbitals have no guaranteed relationship with the quasiparticle amplitudes. However, for many systems, DFT orbitals have been used to successfully reproduce experimental observations.

DFT solves a noninteracting system, and to connect to excited-state phenomena it is necessary to correct the Kohn-Sham orbitals. The full, interacting Green's function can be separated into a noninteracting Green's function and the sum of all connected interaction diagrams called the irreducible self-energy Σ:

$$G = G^0 + G^0 \Sigma G. \tag{1}$$

Following the prescription of Hedin, the many-body interactions are treated within the GW approximation $\Sigma = iGW$ [10].

The DFT exchange-correlation functional can be thought of as an initial approximation to the self-energy. Taking the Kohn-Sham orbitals to be close to the true electron wave functions, the GW corrections can be applied as a complex-valued correction $\Delta\Sigma$ to the LDA energy E^{LDA}, i.e., lowest-order perturbation theory,

$$\begin{aligned} E^{\mathrm{QP}}_{n\mathbf{k}} - E^{\mathrm{LDA}}_{n\mathbf{k}} &= \Delta\Sigma_{n\mathbf{k}} = \langle n\mathbf{k}|\hat{\Sigma}\left(E^{\mathrm{QP}}_{n\mathbf{k}}\right) - \hat{V}_{\mathrm{XC}}|n\mathbf{k}\rangle, \\ \Delta\Sigma_{n\mathbf{k}} &= \Delta E^{GW}_{n\mathbf{k}} + i\Gamma_{n\mathbf{k}}, \end{aligned} \tag{2}$$

where n and $\mathbf{k}$ are the band and crystal momentum of the state. The self-energy operator $\hat{\Sigma}$ depends on the energy of the quasiparticle, and the contributions from the exchange-correlation potential $\hat{V}_{\mathrm{XC}}$ must be subtracted. In insulators, the real part of the self-energy correction ΔE^{GW} generally increases the band gap and stretches both the valence and conduction bands away from the Fermi level. Typically, the corrections can take the form of a static shift and 3% to 5% stretch [11].

The imaginary part of the self-energy $\Gamma_{n\mathbf{k}}$ starts off near zero and in most materials grows smoothly in magnitude with increasing distance from the Fermi level. This imaginary component is related to the physical lifetime. Consider the propagator for a single state n, dropping the spatial dependence,

$$G(\omega) \propto \left[\omega - \left(E^{\mathrm{LDA}}_n + \Delta E^{GW}_n + i\Gamma_n\right)\right]^{-1}. \tag{3}$$

This can be be transformed to the time domain giving

$$G(t - t_0) \propto e^{-i\left(E^{\mathrm{LDA}}_n + \Delta E^{GW}_n\right)(t-t_0)} e^{-\Gamma_n (t-t_0)}, \tag{4}$$

which decays with a characteristic time Γ_n. Single-electron excitations in an interacting system will have finite lifetimes after which they will have scattered into other states. The growth of the imaginary part of the self-energy with increasing separation from the Fermi energy reflects the growth in available states to scatter into. Large discontinuities from this trend do occur, especially for the inner core levels whose lifetime may be longer than much less-bound states deep in the valence band. This is primarily due to differences in the matrix elements for the transition—the core level electrons are much more spatially localized.

Alternatively, the lifetime can be thought of from a scattering perspective, such as in recent work on Auger recombination rates of valence excitations in nitrides [12]. A quasiparticle can only decay if there is an available state to decay into and a way for the scattering process to conserve energy and momentum. In condensed systems, both phonon and photon coupling will allow a quasiparticle to shed energy and momentum, but these contributions are smaller than electron-electron scattering and are neglected by our self-energy calculations. For example, a quasihole i will have a lifetime

$$\frac{1}{\tau_i} \approx \sum_{v,c,f} |\langle i,v|W|f,c\rangle - \langle i,v|W|c,f\rangle|^2 \delta(\epsilon_{vc} + \epsilon_{if}), \tag{5}$$

where v and c are electrons in the valence and conduction bands, respectively, f are possible final hole states, energies ϵ_{vc} are differences in single-particle energies $\epsilon_v - \epsilon_c$, and W is the screened Coulomb operator. More completely, the electron-hole excitation would include excitonic binding, shifting the single-particle energies.

B. X-ray spectroscopy with OCEAN

The OCEAN package can be used to calculate x-ray spectroscopy, including x-ray absorption (XAS), nonresonant inelastic scattering (NRIXS) [also called x-ray Raman scattering (XRS)], x-ray emission (XES), and resonant inelastic x-ray scattering (RIXS) [8,9]. Its primary focus is near-threshold calculations: absorption at or just above the edge or emission from the valence bands. In what follows, there are two important approximations. Firstly, we will not attempt to solve the full many-electron problem. Instead, we use single-particle states and operators. These states are quasiparticles either directly from DFT or with GW corrections. Secondly, we assume that the atomic and electronic degrees of freedom are separable, following the Born-Oppenheimer approximation. The cross-section σ is implicitly dependent on all of the atomic positions $\sigma_{\mathbf{R}}$.

1. Absorption

In OCEAN the Bethe-Salpeter equation is used to account for excitonic effects between the photo-electron and the core hole [13]. The excited-state Hamiltonian is described by two interaction terms: the screened Coulomb attraction W and the bare exchange V_X, which also defines the two-particle propagator $G^{(2)}$,

$$\begin{aligned} H_{\mathrm{BSE}} &= H_0 + V_X - W, \\ G^{(2)}_{\mathrm{BSE}}(\omega,\mathbf{q}) &= [\omega - H_{\mathrm{BSE}}(\mathbf{q})]^{-1}, \end{aligned} \tag{6}$$

where the momentum dependence $\mathbf{q}$ is implicit in the terms of the Hamiltonian. The absorption cross-section can be written

$$\begin{aligned} \sigma(\omega,\hat{\epsilon},\mathbf{q}) &= \frac{2\pi}{q^2}\sum_f |\langle i|\hat{d}^\dagger_{\hat{\epsilon},\mathbf{q}}|f\rangle|^2 \delta(E_f - E_i - \omega) \\ &= \frac{-1}{q^2}\mathrm{Im}\langle i|\hat{d}^\dagger_{\hat{\epsilon},\mathbf{q}}\, G^{(2)}_{\mathrm{BSE}}(\omega,\mathbf{q})\, \hat{d}_{\hat{\epsilon},\mathbf{q}}|i\rangle, \end{aligned} \tag{7}$$

where i denotes the ground state of our system, E_i (E_f) is the energy of the initial (final) state, and the electron-photon operator is $\hat{d} = (\hat{\epsilon}\cdot\mathbf{r})\,(1 + i/2\,(\mathbf{q}\cdot\mathbf{r}) + \mathcal{O}[(\mathbf{q}\cdot\mathbf{r})^2])$.

To evaluate the matrix elements of our BSE Hamiltonian, we consider the space of two-particle states containing one core hole and one conduction-band state. These basis states are eigenstates of the ground-state system, i.e., without the core hole, calculated using DFT with GW corrections. By construction, we conserve the crystal momentum $\mathbf{k}$ such that the electron state is offset from the core hole by the photon's momentum $\mathbf{q}$. For nitrogen $1s$ absorption or emission, the photon momentum and core-hole radius are both small, $\mathbf{q}\cdot\mathbf{r} \ll 1$, and so we use the dipole approximation $\hat{d} = \hat{\epsilon}\cdot\mathbf{r}$. The use of ground-state orbitals for our calculation means that supercells are not required in our approach. However, large cells are necessary to consider disordered systems.

Typically, we make no attempt to directly invert the two-body BSE Hamiltonian, but instead we use the Haydock inversion scheme to approximate the spectrum as a continued fraction [14,15]. In the Haydock approach, the Hamiltonian must be Hermitian, and the quasiparticle lifetimes are applied as a uniform broadening parameter. For near-edge x-ray spectra, the lifetime broadening of the core hole is ordinarily large compared to that of the conduction or valence bands, and therefore the broadening term is constant and this approximation holds. However, if the conduction band lifetimes are not negligible or the core-hole lifetime is variable, as in the case for $L_{2,3}$ edges [16], an alternate method must be used.

For a given incident photon energy ω, we can define the exciton (photoelectron–core-hole pair) as a sum over intermediate states, weighted by the resonant energy denominator and broadened by Γ_m, the lifetimes of both the excited photoelectron and the core hole,

$$|y_{\hat{\epsilon},\mathbf{k}}(\omega)\rangle \equiv \sum_m \frac{|m\rangle\langle m|\hat{d}_{\hat{\epsilon},\mathbf{k}}|i\rangle}{\omega - E_{mi} + i\Gamma_m} = (\omega - \hat{H})^{-1}\hat{d}_{\hat{\epsilon},\mathbf{k}}|i\rangle, \tag{8}$$

where the states $|m\rangle$ are electron-hole pairs involving the ground-state conduction bands, E_{mi} is the energy difference between the excited state m and the initial state i, and the Hamiltonian is the BSE-derived Hamiltonian from Eq. (6). We iteratively solve for $|y(\omega)\rangle$ using an adaptation of the generalized minimal residual (GMRES) algorithm [15,17]. Substituting Eq. (8) into Eq. (7), the absorption spectra become

$$\sigma(\omega,\hat{\epsilon},\mathbf{q}) = -q^{-2}\,\mathrm{Im}\langle i|\hat{d}^\dagger_{\hat{\epsilon},\mathbf{q}}|y_{\hat{\epsilon},\mathbf{k}}(\omega)\rangle, \tag{9}$$

which must then be solved for each frequency point ω to build a spectrum.

2. Resonant inelastic x-ray scattering

In OCEAN, RIXS calculations are carried out analogously to the experimental procedure; the excitation energy is fixed, and then the emission spectrum is determined [18]. First, the incoming x ray excites the system into an intermediate state m, and then the core hole decays radiatively, leaving the system in some final state f. Nonradiative decays are also possible and, for low-Z nuclei like nitrogen, much more prevalent than radiative decays. They were neither measured nor simulated in this work, but they determine a minimum lifetime broadening. The RIXS process is second-order in the Kramers-Heisenberg expansion

$$\begin{aligned} &\sigma(\omega,\hat{\epsilon},\mathbf{k};\omega',\hat{\epsilon}',\mathbf{k}') \\ &\propto \sum_f \left| \sum_m \frac{\langle i|\hat{d}^\dagger_{\hat{\epsilon},\mathbf{k}}|m\rangle\langle m|\hat{d}_{\hat{\epsilon}',\mathbf{k}'}|f\rangle}{\omega - E_{mi} + i\Gamma_m} \right|^2 \delta(E_f - E_i + \omega' - \omega), \end{aligned} \tag{10}$$

where we are now considering a two-photon process, and each photon has an energy, polarization, and momentum $\omega,\hat{\epsilon},\mathbf{k}$ ($\omega',\hat{\epsilon}',\mathbf{k}'$). A strict accounting in powers of the electron-photon interaction A would suggest that we should include two additional terms. The first, A^2, is the NRIXS term, while the second comes from exchanging the absorption and emission vertices [19]. Both lack the resonant energy denominator in the intermediate state of Eq. (10) and are not calculated here.

Taking a cue from experiment, we set the incoming x-ray energy ω by first solving for the intermediate state exciton $|y(\omega)\rangle$ using the GMRES. Substituting Eq. (8) into Eq. (10),

the RIXS cross section becomes

$$\sigma(\omega,\hat{\epsilon},\mathbf{k};\,\omega',\hat{\epsilon}',\mathbf{k}') \propto \sum_f |\langle y_{\hat{\epsilon},\mathbf{k}}(\omega)|\hat{d}_{\hat{\epsilon}',\mathbf{k}'}|f\rangle|^2\delta(E_{fi}-\Omega)$$

$$\propto \mathrm{Im}\langle y_{\hat{\epsilon},\mathbf{k}}(\omega)|\hat{d}_{\hat{\epsilon}',\mathbf{k}'}\,G^{(2)}_{\mathrm{BSE}}(\Omega,\mathbf{q})\,\hat{d}^{\dagger}_{\hat{\epsilon}',\mathbf{k}'}|y_{\hat{\epsilon},\mathbf{k}}(\omega)\rangle, \tag{11}$$

where now the Green's function involves a valence-conduction electron-hole pair and depends on energy loss $\Omega=\omega-\omega'$ and momentum transfer $\mathbf{q}=\mathbf{k}-\mathbf{k}'$ between the initial and final x rays. The core hole is filled when the out-going x ray is emitted, and therefore this final state is made up of a valence-band hole and conduction-band electron. For this final step, we use a modified version of the valence (UV/Vis) BSE package AI2NBSE [20]. Once again, when the electron and (valence) hole lifetimes can be approximated by a constant, the Haydock scheme can be used to generate the full spectra as a function of the energy loss Ω. Similarily, the GMRES algorithm can be used when variations in the state-dependent lifetime broadening are important by defining the final conduction-valence exciton

$$|\tilde{y}_{\hat{\epsilon},\mathbf{k},\hat{\epsilon}',\mathbf{k}'}(\omega,\omega')\rangle = (\Omega-\hat{H})^{-1}\hat{d}^{\dagger}_{\hat{\epsilon}',\mathbf{k}'}|y_{\hat{\epsilon},\mathbf{k}}(\omega)\rangle, \tag{12}$$

which depends upon both the incoming and outgoing x rays. Inserting Eq. (12) into Eq. (11) gives

$$\sigma(\omega,\hat{\epsilon},\mathbf{k};\omega',\hat{\epsilon}',\mathbf{k}') \propto \mathrm{Im}\langle y_{\hat{\epsilon},\mathbf{k}}(\omega)|\hat{d}_{\hat{\epsilon},\mathbf{q}}\,|\tilde{y}_{\hat{\epsilon},\mathbf{k},\hat{\epsilon}',\mathbf{k}'}(\omega,\omega')\rangle. \tag{13}$$

Including valence excitonic effects per Eq. (11) shifts spectral weight toward higher emission energies (lower loss), reflecting the valence-hole–conduction-electron excitonic binding [21–23]. This effect is more pronounced at lower initial excitation energies where the photo-electron remains more localized. If we neglect electron-hole interactions in both the intermediate and final states, the result is equivalent to treating RIXS as a convolution of occupied and unoccupied densities of states [24]. Nonresonant XES has long been treated as the occupied density of states projected onto the core hole, and experimentally RIXS is seen to approach the nonresonant limit within about 20 eV of threshold. The nonresonant condition can be defined in experiment as the point after which subsequent changes in incident photon energy have no effect on the emitted spectrum.

Several effects contribute to the cross-over from resonant to nonresonant emission. The final state in Eq. (11) does not include a core hole, and so contributions from every core hole are included in the coherent sum over intermediate states. Phonon scattering events can degrade the resulting interference effects by providing large momentum transfer at very small energy loss as compared to the electronic transitions, and therefore they can decouple the momenta of the core-hole and conduction-electron prior to x-ray emission [23,25]. Other mechanisms such as multiple excitations, the creation of additional valence excitons or plasmons at higher excitation energies, also contribute to the loss of interference effects. Lastly, at high energies, the conduction-band states asymptotically approach free-electron states and the bands become flat and dense, eliminating any **k** space selectivity in the absorption matrix elements. Of these three factors, only the final one is included in our calculations.

3. Edge alignment

Our approach described so far lacks an absolute energy alignment. The DFT calculations are done using pseudopotentials, which lack 1*s* states. However, following previous, DFT-based spectroscopy investigations we reduce this free parameter to a single calibration [1,26–28]. We compensate for the changed chemical environment around the nitrogen core-hole site and for each site calculate the 1*s* energy

$$\epsilon_{\mathrm{N}1s} = \Delta\epsilon_{\mathrm{N}1s} + 1/2\,W(\tau_{\mathrm{N}}) + V_{\mathrm{KS}}(\tau_{\mathrm{N}}), \tag{14}$$

where W is the screened Coulomb potential of the core hole and V_{KS} is the total Kohn-Sham potential, both evaluated at the core-hole site τ. The remaining term $\Delta\epsilon$ is the calibration term, which depends on the details of the psuedopotential and the size of the unit cell. A single value of $\Delta\epsilon$ is used for all of the snapshots. While not as satisfying as an *ab initio* calibration, this approach is sufficient to compare various configurations of crystalline materials.

C. Vibrational disorder

In crystalline systems, even those approaching 0 K, the ions are vibrating around their equilibrium positions. For an extended x-ray absorption fine structure (EXAFS), this disorder is parameterized as the Debye-Waller (DW) factor [29]. In EXAFS, the DW term captures the broadening of peaks caused by the imperfect spacing of the vibrating atoms. Analogously in RIXS, variations away from a perfect crystal lead to a breakdown of the coherence, which can be parameterized into a temperature-dependent DW factor that mixes in some nonresonant emission [30]. However, in the near-edge, vibrational disorder can also lead to qualitative changes which cannot be captured by the DW factor, such as the observation of so-called dark states which would be dipole forbidden in the undistorted structure [31]. The OCEAN code treats the ions as fixed during the x-ray excitation process, but the effects of vibrational disorder can be considered by taking an average over an appropriate ensemble of structures. For very short core-hole lifetimes the ions will not have time to react to changes in electrostatic potential due to the core hole, and the correct ensemble can be constructed from the finite-temperature ground-state phonon distribution. In this work, we take the approximation that the atoms are stationary on the time scale of the core-hole lifetime.

Ionic disorder can be modeled in several ways. Most simplistically, uncorrelated disorder can be added by way of distributing the ions according to their thermal parameters, as determined by x-ray or neutron scattering experiments. Molecular dynamics (MD) simulations are widely used, whereby several snapshots are used as structures for calculations. This approach is straightforward, and it has the advantage of providing physical insight into the behavior of a system, e.g., the dynamics of supported nanostructures [32]. However, the nuclei in MD simulations are treated classically, and molecular solids have a significant number of very high-frequency vibrational modes associated with intramolecular motion. These modes can be in the 1000 to 3000 cm^{-1} range or some 5 to 15 times $k_{\mathrm{B}}T$ at room temperature, and therefore they may be poorly sampled by standard MD. Path integral

molecular dynamics includes the quantum behavior, but at a greatly increased computational cost [33,34].

Previously, we introduced an alternate approach for generating an ensemble of structures based upon populating the phonon modes of the system [1]. Our method is designed for crystalline systems where the ions have well-defined centroid positions around which they vibrate. It requires only modest computational cost and can be used to explore temperature dependence at no significant additional cost. Briefly, phonon modes are calculated using density-functional perturbation theory (DFPT) as implemented in the QUANTUM ESPRESSO package [35]. In Sec. III C 1, we review constructing phonon modes using DFPT within the harmonic approximation; in Sec. III C 2, we outline our procedure for creating snapshots; and in Sec. III C 3, we discuss some limitations of our approach.

1. Harmonic approximation

The interatomic forces are assumed to be harmonic, such that the vibrational system can be fully defined by the matrix of force constants

$$F_{i\epsilon,j\epsilon'}(\mathbf{R}-\mathbf{R}') = \frac{\partial^2 E}{\partial u_{i\epsilon}(\mathbf{R})\partial u_{j\epsilon'}(\mathbf{R}')}, \tag{15}$$

where $u_{i\epsilon}(\mathbf{R})$ [$u_{j\epsilon'}(\mathbf{R}')$] is the displacement of ion i (j) in direction $\hat{\epsilon}$ ($\hat{\epsilon'}$) and cell $\mathbf{R}$ ($\mathbf{R}'$). The calculation of the force constants is carried out in reciprocal space on a uniform mesh $\mathbf{q}$. The force constants have limited real-space range, dying off as $|\mathbf{R}-\mathbf{R}'|$ increases, and therefore Fourier interpolation can be used to generate a much denser $\mathbf{q}$-mesh without explicit calculation. We refer the reader to Ref. [35] and references therein. The dynamical matrix is defined from the force constants

$$D_{i\epsilon,j\epsilon'}(\mathbf{q}) = \frac{F_{i\epsilon,j\epsilon'}(\mathbf{q})}{(M_i M_j)^{1/2}}, \quad D(\mathbf{q})\vec{\xi}_{\lambda,\mathbf{q}} = \omega^2_{\lambda,\mathbf{q}}\vec{\xi}_{\lambda,\mathbf{q}}, \tag{16}$$

which can be diagonalized to give the phonon modes ξ and frequencies ω.

To build up a representative set of structures, we first note that we have assumed that the ions are moving in harmonic potentials. Therefore the probability density of a given ion i moving in mode $\lambda,\mathbf{q}$ can be given by a normal distribution with variance

$$\langle u^2(T)\rangle_{i\lambda\mathbf{q}} = \frac{|\vec{\xi}_{i,\lambda,\mathbf{q}}|^2}{M_i\omega_{\lambda,\mathbf{q}}}(1/2 + n(\omega_{\lambda,\mathbf{q}};T)), \tag{17}$$

where $n(\omega_{\lambda,\mathbf{q}};T) = [e^{\omega_{\lambda,\mathbf{q}}/k_B T}-1]^{-1}$ is the Bose occupation number which varies with temperature T, and k_B is Boltzman's constant. The probability that an ion i will be displaced by some amount $\Delta\tau$ along its phonon trajectory $\xi(x)$ is then simply

$$P_{i,\lambda,q}(\Delta\tau;T) = \frac{1}{\sqrt{2\pi}\,u}\, e^{-\Delta\tau^2/2u^2_{i\lambda\mathbf{q}}(T)}. \tag{18}$$

The factor of $1/2$ in the variance is the zero-point motion—for a quantum harmonic oscillator the lowest state has finite extent, which for light nuclei can be significant. For example, the symmetric breathing mode of the hydrogen atoms in NH_4NO_3 has a calculated frequency of $\approx$3000 cm^{-1}, which has negligible occupation at room temperature. However, the zero-point motion of this mode gives each hydrogen a standard deviation of 0.1 a.u., $\pm$5% of the NH bond length.

2. Building snapshots

We construct structures by perturbing the system with noise. For each structure, we take a set of random numbers $\{g\}$ according to the probability distribution calculated in Eq. (18) for that mode. The total displacement of atom i in cell $\mathbf{R}$ in each direction $\hat{\epsilon}$ is

$$\Delta\tau_{\hat{\epsilon},i,\mathbf{R}}(T) = \sum_{\mathbf{q}}\sum_{\lambda}\frac{g_{\mathbf{q},\lambda}}{\sqrt{N_{\mathbf{q}}}}e^{i\mathbf{q}\cdot\mathbf{R}}\,\vec{\xi}_{\lambda,\mathbf{q}}\cdot\hat{\epsilon}. \tag{19}$$

Note that the amplitude g assigned to each mode is shared by every atom in the supercell. In this way, the disorder is correlated by mode, e.g., in the aforementioned hydrogen breathing mode all four hydrogen atoms would be displaced by the same amount. Each structure is the result of its own set of random numbers $\{g\}$, and by summing the spectra of many structures together we create an average calculated spectrum that can be compared to the observed spectrum.

3. Limitations

Our approach is designed for crystals where each atom is in a stable minimum of the potential energy surface. This excludes liquids or crystals near a phase transition where the atomic positions may in fact be on saddle points. This method also assumes that the phonon modes remain harmonic and independent for all atomic displacements that are probed by the disorder. These drawbacks could be mitigated by including cubic and quartic corrections to the potential energy surface of each phonon mode. In addition, cross terms between modes will enter in at the same order in mode displacement as the quartic term, complicating the approach.

For very large structures, calculating phonon modes with DFPT is not feasible as the computational cost grows with the third power of the number of atoms [35]. Instead, a limited force constant matrix can be constructed in real-space by analyzing molecular dynamics or Monte Carlo simulations [36]. While, in principle, this alternate method could be substituted into our workflow, this work only concerns quite small unit cells, and we have not investigated an appropriate cross-over from reciprocal- to real-space methods for calculating the force constants.

IV. RESULTS

Ammonium nitrate can be thought of as a binary ionic crystal with an electron transferred from the NH_4^+ to the NO_3^-. At ambient conditions it forms a *Pmmn* crystal structure. The planar nitrate ions are aligned in layers, resulting in a well-defined anisotropy in the electronic response. However, our experimental data were taken on a powdered sample, and so both the measured and calculated x-ray spectra are averaged over polarizations. We checked that including quadrupole terms in the transition operator had no effect on the calculated spectra, and therefore only the dipole term was included in the calculations shown here.

A. Electronic structure

We used the ABINIT DFT package [37] to carry out self-energy calculations of NH_4NO_3 using the experimentally determined atomic coordinates and lattice parameters [38] and the local-density approximation (LDA) as parameterized by Ceperley/Alder Perdew/Wang [39]. We used a Γ-centered 4^3 **k**-point grid, and, because we are interested in the behavior of the full valence band, we used contour deformation for calculating the self-energy. We self-consistently updated the energies of the Kohn-Sham orbitals, but held the orbitals themselves constant. Typical of GW calculations, the screening is calculated within the random phase approximation. As was noted previously, the NO σ bonds in NH_4NO_3 have a large amount of self-energy broadening that is clearly evident in the XES [1].

We show the GW-corrected band structure for ammonium nitrate in Fig. 1. Wannier orbitals were constructed from hydrogenic states using the WANNIER90 code [40] so that the nitrogen p-type orbitals could be projected onto the band structure. Each band is colored based upon the overlap with p-type states on either the nitrate nitrogen or on the ammonium nitrogen. Bright, blue states are majority nitrate based, whereas bright orange is associated with a strong contribution from the ammonium. The light grey states have little contribution from either, whereas darker states have both.

Starting from the most-bound, the N_{NO_3} $2s$ states (not pictured) form a flat band at -31 eV. Around -23.5 eV are clustered four NO σ bands and two N_{NH_4} $2s$ states. While the LDA calculation gives a clear 1.5 eV separation between them, after GW corrections they are nearly degenerate. The s-type states are dipole forbidden in Kα emission and are therefore not present in the spectra. The main contributions to the emission come from the cluster of bands between -10 and -13 eV. In the core-level spectroscopy, however, the two inequivalent nitrogen sites have very different chemical shifts, and the NH_4-derived peak is in fact observed some 4 to 5 eV lower in energy than the NO_3 contribution. The ammonium $2p$ states are relatively isotropic and show little **k** dependence. In contrast, the NO_3 π states have distinct hotspots in the Brillioun zone. Lastly, the least-bound cluster of bands between -5 and -3 eV are primarily delocalized oxygen $2p$-type states which contribute a small peak to the nitrogen K_α emission.

The conduction band picture is complicated, and caution must be used when comparing it to x-ray absorption, as the band structure only reflects the ground state. The strong, local core-hole potential will selectively pull down states near the excitation site. With that disclaimer, we have included the lowest sixteen conduction bands in Fig. 1. The LUMO and LUMO+1 are primarily associated with the nitrate ion and lead to the strong exciton peak in the XAS. While the first bands with ammonium p-type character are much higher into the conduction band, the same chemical shift that affects the emission brings their contribution to the XAS much closer in energy to that of the nitrate.

As previously noted, the NO σ bonds have a very large, 1.1 eV, imaginary self-energy (short quasiparticle lifetime) [1]. In Fig. 2 (top), it is clear that this effect is unique to the NO σ bands. The nearby N_{NH_4} $2s$ states ($E^{\mathrm{LDA}} = -18.3$ eV) have

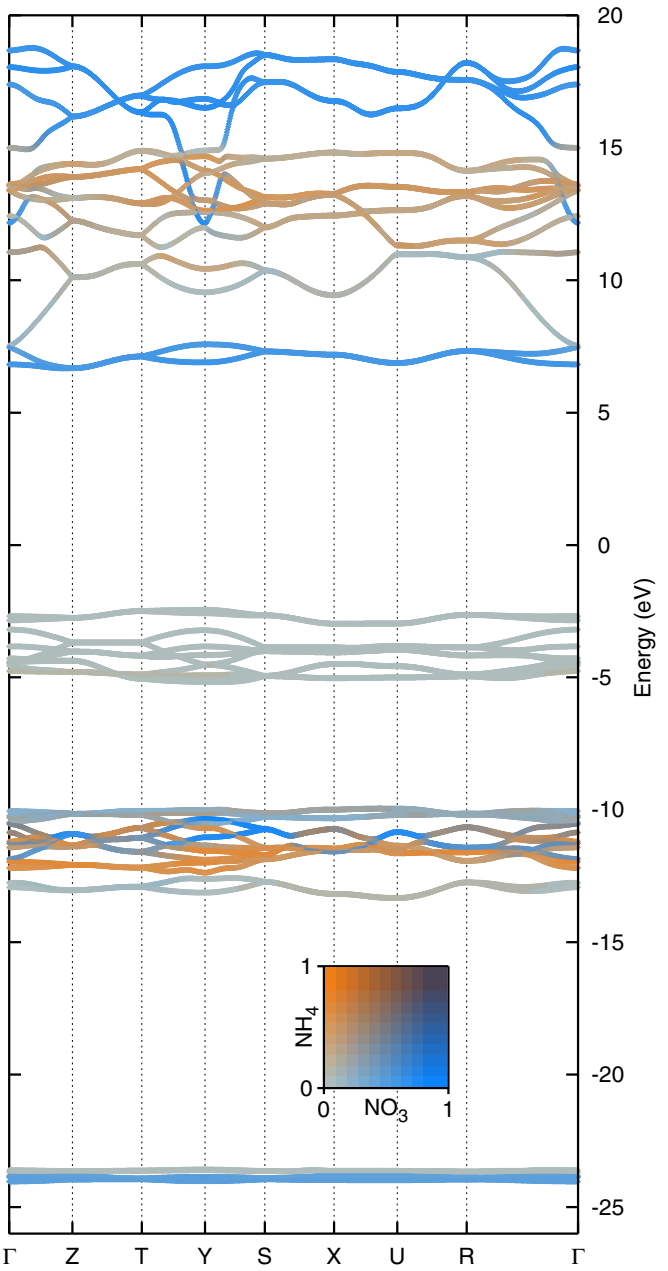

FIG. 1. The GW band structure of NH_4NO_3. The coloring (inset) is by overlap with bright orange states being primarily p-type states on the nitrogens, which make up the ammonium, and the bright blue belonging to p-type states on the nitrate. Light grey bands either have s-type character or have little overlap with the nitrogen atoms.

a broadening that is only around 0.1 eV. Coincidentally, the GW corrections give nearly the same quasiparticle energies for the N_{NH_4} s and NO σ states. For reference, the oxygen and nitrogen $1s$ states have measured lifetime broadenings of approximately 0.1 eV, around ten times smaller (longer-lived) than the σ states. This is set by Auger decays. To explain this state-specific short lifetime, we note two factors imposed by Eq. (5) (as in any transition probability): energy conservation and matrix elements. Figure 2 (bottom) shows the $l = 1$ projected densities of states for both nitrogen sites. On the nitrate-centered nitrogen, the gap between the π and σ orbitals

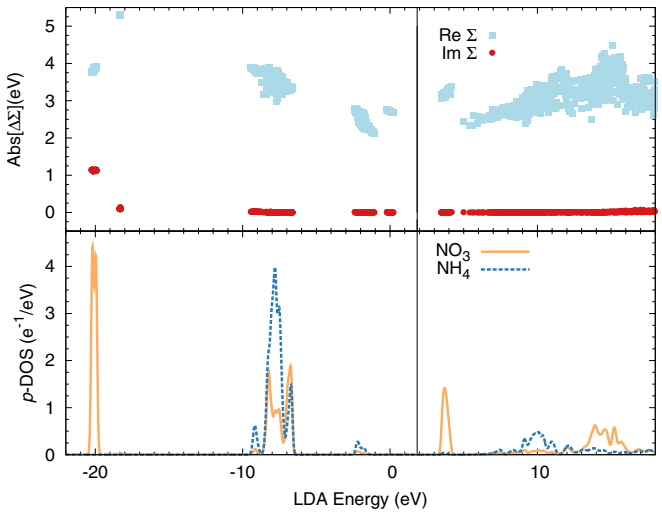

FIG. 2. (Top) The absolute values of the real (light-blue squares) and imaginary (red circles) components of the self-energy corrections as a function of the LDA energy for the valence and low-lying conduction bands of ammonium nitrate. (Bottom) The projected local densities of states (p-DOS) for $l = 1$ around the nitrate-centered (orange, solid) and ammonium-centered (blue, dashed) nitrogen atoms. Only the NO σ bonds near -20 eV show an imaginary self-energy that varies significantly from zero. The black vertical line marks the middle of the band gap.

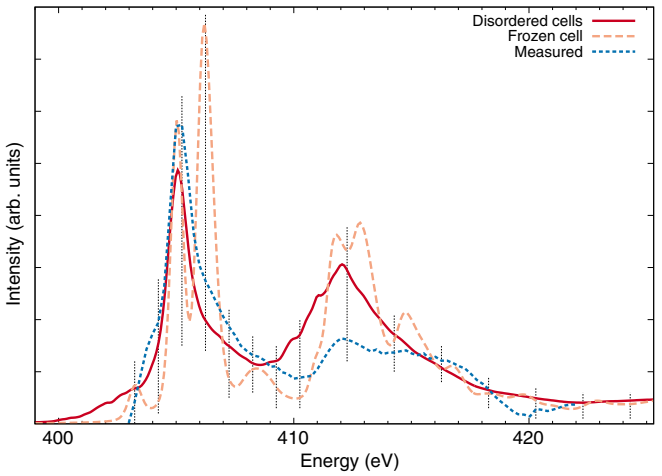

FIG. 3. The nitrogen K-edge absorption comparing theory and experiment. The effect of vibrational disorder is notable in going from a calculation using the "frozen" coordinates to one including disorder. This is especially true for the NH_4 exciton around 407 eV in the absorption. The main NO_3 peak at 405 eV is less affected by vibrational broadening.

is larger than the GW band gap of 9.0 eV. The localization of these molecularlike states, both σ and π, combined with their favorable energy spacing leads to extremely short quasihole lifetimes due to what are effectively Coster-Kronig Auger decays of the NO σ states.

B. X-ray spectra

The calculated spectra are averages over an ensemble of 15 structures including vibrational disorder [1]. The structures were created from $2 \times 2 \times 2$ supercells using the method outlined in Sec. III C. For the x-ray spectra calculated in this work, we have used orbitals from the plane-wave DFT package QUANTUM ESPRESSO [42]. Our calculations use pseudopotentials, and so an auxiliary atomic code and pseudopotential inversion scheme are necessary for core-level spectroscopy [8]. Electron orbitals are calculated on a regular grid in the Brillouin zone $|\psi_{n,\mathbf{k}}\rangle = e^{i\mathbf{k}\cdot\mathbf{r}}|u_{n,\mathbf{k}}\rangle$, and overlap integrals are carried out by summing over this grid. To accelerate convergence we use a symmetry-breaking shift [15] and an adaptation of the $\mathbf{k}$-space interpolation scheme of Shirley as extended by Prendergast and Louie [43,44]. We found a $2 \times 2 \times 2$ $\mathbf{k}$-point grid to be sufficient such that increasing the number of $\mathbf{k}$ points would have no discernible effects on the resulting spectra.

The cost of carrying out GW calculations for 15 supercells was considered to be prohibitive. Instead we incorporated the self-energy corrections by making several approximations. First, we note that the lifetime broadening of the conduction band remains small through the region of interest (<20 eV above the Fermi level) and can be neglected. The real part of the self-energy correction for the conduction bands can be captured using a static shift, i.e., scissor operator. The valence band states are more complicated with energy-dependent real and imaginary self-energy corrections, but the occupied states can be separated into various groups by their DFT energies (Fig. 2). Within each group the GW corrections are relatively uniform. This uniformity within well-separated groups means the corrections can be averaged over $\mathbf{k}$ points to give a correction $\Delta\Sigma_n$ that is a function of band only. While we include the effects of disorder through the DFT calculations of each supercell, we assume that variations in the GW corrections from disorder should be small and calculate $\Delta\Sigma_n$ only for the ordered cell using the GW calculation from the previous section.

1. X-ray absorption

The measured and calculated nitrogen K-edge XAS of ammonium nitrate are shown in Fig. 3. In addition to the disordered cell, we also show the spectrum from a cell with all the atoms frozen at their average positions. The disordered cells include 0.1 eV broadening from the core hole lifetime, while the frozen cell also includes an additional 0.5 eV Gaussian broadening. The effect of including disorder is dramatic. Specifically, the NH_4 exciton is sharp and distinct when using the "frozen" configuration, but becomes smeared out and almost indistinguishable once vibrations are taken into account. In contrast, the NO_3 exciton remains sharp, and most of its apparent broadening is from the ammonium peak widening and contributing to spectral strength below the nitrate peak. The addition of disorder adds peak dependent broadening with little change in total spectral weight.

The calculated and measured absorption spectra have several differences. The most notable variance is the relative intensities of the main exciton at 405 eV versus the higher-energy features from 411 to 418 eV. Some of this discrepancy arises from difficulties in converting from the measured partial fluorescence yield to absorption. The short mean free path of

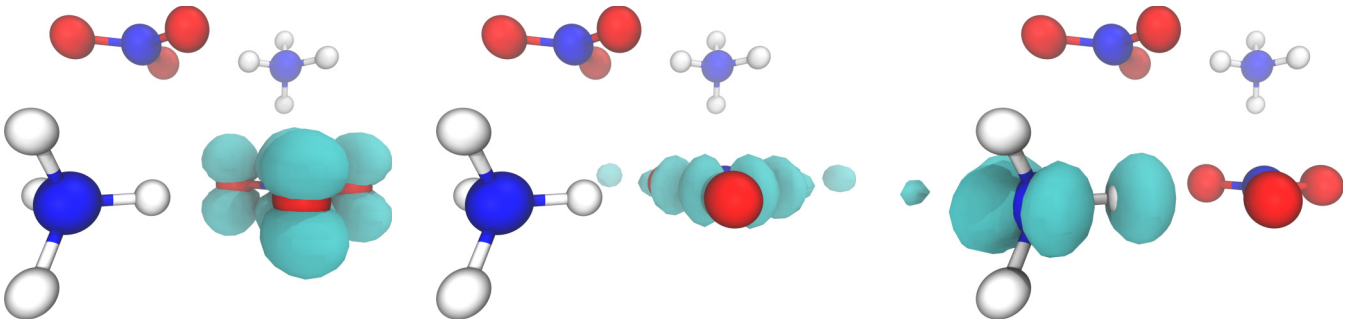

(a) (b) (c)

FIG. 4. Electron density plots of the NO_3 (a) and (b) and NH_4 (c) excitons are shown for select excitation energies andpolarizations (plotted using VMD [41]). The nitrate exciton at 405 eV protrudes into the open space above and below the nitrate plane—whereas the ammonium exciton at 406.6 eV encompasses the hydrogen atoms and in turn is quite sensitive to the large vibrational displacements that the hydrogen atoms undergo. The higher energy NO_3 σ^* exciton (412.8 eV) is also strongly in uenced by vibrational disorder.

both the incident and out-going (fluoresced) x rays results in strong self-absorption effects, and the final peak intensities are very sensitive to the details of the self-absorption corrections. More subtly, our calculation method overbroadens the ammonium peak, reducing the apparent spectral weight of the main exciton. This gives rise to the spurious spectral weight below the edge (400 to 403 eV), and is more evident when only the NH_4^+ ion is present such as in NH_4Cl [1]. The feature around 417 eV in experiment, missing in the calculation, may be an artifact of the aforementioned difficulties in processing the measurements, or it may arise from multielectron excitations not included in the calculation.

The significant difference in behavior between the nitrate and ammonium excitons originates in the differences between the excitons' shapes and overlaps with the atoms in the crystal. By using Eq. (8), we can solve for the excitonic wave function as a function of energy and plot the exciton's electron density in real-space around the core hole. Using the "frozen" configuration we solved for the excitonic wave functions associated with an ammonium-centered (406.6 eV) and a nitrate-centered (405.1 eV) nitrogen hole, and the resulting electron densities are shown in Figs. 4(a) and 4(c), respectively. At 405.1 eV, only x-rays polarized along the c axis have any spectral weight, while the ammonium exciton at 406.6 eV is nearly degenerate for $\hat{x}$, $\hat{y}$, or $\hat{z}$ polarizations; we show only a single polarization. We have also included a higher-energy nitrate feature at 412.8 eV with $\hat{\epsilon} = \hat{x}$.

The lowest nitrate exciton extends above and below the NO_3 plane into relatively empty spaces. Hence it is mostly unaffected by the relative motion of the nitrogen and oxygen constituents of the nitrate. In contrast, the ammonium exciton encompasses the hydrogen atoms, and will be strongly affected by changes in the NH bond lengths or angles. Compounding this sensitivity to the relative hydrogen locations, their small atomic mass leads to correspondingly larger displacements of the hydrogen atoms away from their equilibrium positions. The higher-energy nitrate features around 412 eV lie primarily along the NO bonds [Fig. 4(b)], and, like the ammonium peak, are also quite sensitive to intramolecular vibrations.

2. *RIXS*

Resonant inelastic x-ray scattering spectra were obtained at fourteen excitation energies above the nitrogen K edge. Each spectrum was taken with a count time of 4200 s and was normalized to the beam intensity from the monochromator. The spectra were then corrected for self-absorption in the sample at the excitation energy. Spectra were taken at excitation energies 1 eV apart up to 410 eV and 2 eV apart thereafter. The calibrated excitation energies are noted by short vertical lines on the absorption spectrum in Fig. 3. The emission spectra contain two main features that can be identified as arising separately from the ammonium and the nitrate constituents by comparing to previous experiments on compounds containing only one of the two as well as the calculated emission, which can selectively exclude contributions [1]. The ammonium motif is characterized by a broad main feature centered around 388 eV with a smaller shoulder near 394 eV. The nitrate contribution consists of a strong, sharp peak near 394 eV and a very broad feature down at ∼382 eV.

Calculations of the RIXS spectra were carried out on the same ensemble of 15 2^3-supercell structures as the absorption. For each structure, six pairs of incoming and outgoing x-ray polarizations were averaged together. The outgoing x rays are parallel to the incoming beam's polarization, reducing the number of polarization combinations from nine to six. The lifetime of the nitrogen 1s hole was assumed to be 0.1 eV, and, per Eq. (8), this broadening selects intermediate-state excitons with energies near the excitation energy. In nitrogen the 1s hole lifetime is set by the Auger decay rate; for light elements, nonradiative decays are the dominant decay channel for core-hole excitations. The Haydock algorithm in AI2NBSE assumes that the BSE Hamiltonian is Hermitian, and therefore it is incompatible with the complex energies obtained from the GW calculations. To generate the GW-corrected RIXS spectra, we used the same GMRES approach as outlined in Sec. III B 2 within the valence code [15]. Calibration of the calculated emission energy was done once and used for all the RIXS spectra.

A selection of RIXS spectra is shown in Fig. 5. Measured spectra are shown as blue/light blue solid lines while calculations are red/orange dashed lines; colors are alternated

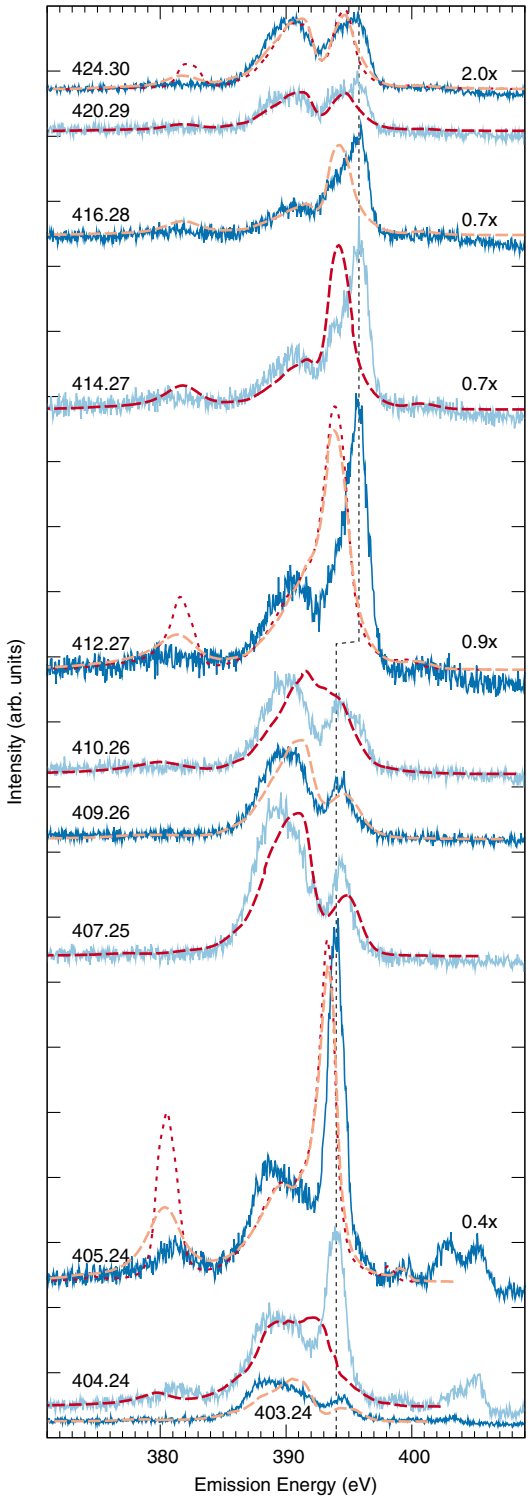

FIG. 5. Measured (blue/light blue, solid) and calculated (red/orange, dashed) RIXS of NH_4NO_3 (see text). Numbers along the left above each set of spectra denote the incident x-ray energy in eV. Spectra are offset vertically and scaled according to the numbers along the right. Measured spectra are normalized for beam intensity and count time and corrected for self-absorption. Calculated spectra are normalized to fit. At 405, 412, and 424 eV, the thin, dotted lines show the calculations without the complex-valued self-energy corrections. The black dashed line indicates a shift in the NO π peak from 394.0 to 395.8 eV with increasing incident energy.

to increase legibility. At several energies—405.24, 412.27, and 424.30 eV—RIXS calculations using LDA energies are shown as red dotted lines in addition to the GW-corrected ones. Emission spectra at different excitation energies are offset vertically for clarity and labeled on the left-hand side by the initial excitation energy. Several spectra have been further scaled as noted by the multiplier on the right-hand side. As the excitation energy is tuned across the main edge, from 403 eV to above 420 eV, the emission undergoes substantial changes. Within the emission there are four main features which correspond to different sections of the band structure (Fig. 2).

The small peak in the emission near 400 eV comes from the bands around -3 to -5 eV transitioning to the nitrate-centered nitrogen. This weak feature is most easily observed at energies where the nitrate contributions are dominant, e.g., 405.24 and 412.27 eV. At an excitation energy of 405.24 eV the inclusion of GW corrections (orange, dashed line) is seen to improve the spacing between of the main nitrate peak and this higher-energy feature compared to the LDA energies (red, dotted). These bands also overlap with the ammonium, but, because of a 4.7 eV chemical shift, features from the ammonium-centered nitrogen have a lower relative emission energy than the band structure otherwise indicates. Therefore emission from these low-lying valence bands to the NH_4-centered 1s hole is hidden by other features in the spectrum at many of the excitation energies. However, near 404, 407, and 409 eV there is little to no contribution from the nitrate, and the emission feature at 394.5 eV (394.8 eV) in the measured (calculated) spectra come from these bands.

The NO_3^- π orbitals, between -10 and -14 eV in the band structure, give rise to a strong peak in the emission around 394 to 396 eV. The rises and falls of this feature with excitation energy provide a clear signal of the nitrate contributions to the x-ray absorption and subsequent emission. The strength of this peak is correlated with the weights of the other two nitrate features, the aforementioned 400 eV feature as well as the NO σ peak around 382 eV. As the excitation energy changes from the exciton at 405 eV to the next grouping of nitrate absorption features from 412 to 416 eV the NO π emission feature is seen to shift by 1.8 eV from 394.0 to 395.8 eV as highlighted by the dashed black vertical guidelines. The calculated emission peaks also shift, but only by 0.9 eV, from 393.4 to 394.3 eV as the incident energy is changed from 405 to 414 eV. We suggest the positioning of the NO_3^- π peak may be influenced by vibrational effects in the intermediate RIXS state which are neglected in our calculation. As the excitation energy is raised to the nonresonant limit, this peak is seen to broaden or show contributions from two, closely spaced peaks, but the calculated emission spectrum shows only a single feature. Emission from the NO_3^- π orbitals has nearly the same emission as from the low-lying valence to the NH_4-centered 1s creating a single combined peak when both have similar strengths, such as at 410 eV.

The main ammonium feature is a broad peak ranging from around 387 to 391 eV, which orginates from NH_4 σ orbitals. The measured spectrum changes little with excitation energy, cf., 403.23 eV versus 407.25 eV. At excitation energies with little contribution from the nitrate such as 403, 407, and 409 eV the higher-energy feature at 394.5 eV comes from overlap with the shallow valence bands. Throughout, the calculated RIXS

underestimates the relative intensity and spacing of this smaller peak. The calculated shape of the main ammonium peak is consistently too high in energy and asymmetric compared with the measured spectra. We attribute these discrepancies to a neglect of vibrational relaxation during the RIXS process which for the light hydrogen atoms could prove significant.

The lowest energy feature in the emission around 382 eV originates from the NO σ bonds. Unsurprisingly, it is strongest at excitation energies that exhibit a strong peak associated with the NO π bonds (though polarized emission spectra would separate these two). The extreme broadening observed in experiment stands in stark contrast to previous XES calculations [45] or the band structure in Fig. 1 which indicates that the NO σ bands have almost no dispersion. RIXS calculations using LDA energies are shown as red, dotted lines for 405.24, 412.27, and 424.30 eV. These show that some broadening of the NO σ band arise from vibrational disorder in the crystal, but it is only after GW-corrected, complex energies are included that the calculations begin to show the sort of broadening observed experimentally (see Fig. 2). However, even including the GW corrections, the calculated NO σ peak is much narrower in the calculation than in experiment. Both measured and calculated spectra show a sharpening of the NO σ peak as the excitation energy is lowered towards the edge, e.g., from 412.27 to 405.24 eV. This is the result of excitonic binding of the final conduction-band electron and valence-band hole.

Our approach neglects the response of the atoms to the sudden creation of a core hole by x-ray absorption. Even though the core hole lifetime is only a few femtoseconds, we expect some relaxation to occur. To test what effects might be seen by incorporating relaxation, we considered 2^3 ordered supercells with one of the nitrogen peudopotentials replaced with a core-hole pseudopotential, i.e., a $1s^1 2s^2 2p^5$ instead of $1s^2 2s^2 2p^4$ configuration, and we allowed the nearest neighbor atoms to relax [46]. With the core hole on the NO_3^- the NO bond distance increased by 0.1 a.u., which caused the emission energy of the NO π peak to increase by 0.8 eV. When instead the core hole was placed on the ammonium the local structure changes dramatically. One of the hydrogen atoms is ejected from the ammonium and binds instead to an oxygen, creating an N^*H_3 and an NO_3H. The NH bond length changes from 2.0 to 3.4 a.u., while the OH bond goes from 3.3 to 1.9 a.u. This change lowers the main NH σ emission peak by 1.5 eV and strengthens the higher-energy secondary peak significantly in addition to lowering it by around 1 eV. For both ammonium- and nitrate-centered core holes, the changes in calculated emission upon relaxation of the neighboring atoms was consistent with reducing the discrepancies between the calculated and measured emission. However, this assumes a very long-lived core hole. A thorough accounting of the excited-state vibrational effects must consider both the influence of the exciton, which may remain very localized near threshold, and the limited lifetime of the core hole, either of which could substantially alter our preliminary results.

V. CONCLUDING REMARKS

We have presented measured and calculated RIXS spectra of the nitrogen K edge in ammonium nitrate. The measured emission shows dramatic changes in features and intensities as the absorption energy is varied. Our Bethe-Salpeter equation approach within the OCEAN code adequately captures the spectral changes seen in experiment, but we note the critical addition of several steps beyond a standard BSE approach for calculating x-ray spectra of crystalline systems was needed.

The first is the need to simulate the intrinsic disorder in the crystal from vibrations (both thermal and zero-point motion). As was shown previously, the effect of vibrational disorder in ammonium nitrate on the nitrogen XAS is dramatic [1]. This is compounded in RIXS calculations where a failure to accurately describe absorption precludes a meaningful emission spectrum. In ammonium nitrate, vibrational disorder changes the near-edge region (below 410 eV) from a highly structured spectrum with two well-separated peaks to one with a sharp nitrate peak overlayed on top of a highly broadened ammonium peak. The measured emission at 403 and 404 eV clearly show this ammonium character, and the OCEAN calculation is able to capture this effect by sampling disordered configurations.

The second important consideration is the effect of the fully complex GW corrections. The substantial many-body lifetime broadening of the NO σ bonds is responsible for the majority of the calculated broadening of their corresponding emission feature with a smaller effect coming from initial-state vibrational disorder. The calculations include this self-energy broadening only at the quasiparticle level which assumes that the spectral function is represented by a Lorentzian distribution $A(\omega) = -\pi^{-1}\Gamma/(\omega^2 + \Gamma^2)$, but for large broadenings, this assumption may be poor. However, going beyond this quasiparticle assumption would require a reformulation of the BSE and is beyond the scope of this work.

Neglected in our calculations to date is any consideration of vibrational relaxations around the core hole or interference effects between intermediate and final-state vibrations. This has been previously investigated in molecular systems with few enough relevant electronic and vibrational degrees of freedom that explicit Hamiltonians can be constructed [47] and also in model systems [25]. Prior work exists for aqueous systems, following the molecular dynamics of the system between the creation of the core hole and its subsequent decay and tracing the effect of the changing structure on the x-ray emission [48,49]. Future work is needed to incorporate this effect into a crystalline, condensed matter framework.

The broadening of the NO σ peak in the emission spectra is attributed to a self-energy effect, which is largely captured within the GW approximation. A reexamination of other x-ray emission and Auger experiments at the nitrogen K edge of nitrate compounds shows that this effect is general across several compounds, though it was not remarked upon until recently [1]. We suggest that this anomalously large lifetime broadening can be understood via a simple interpretation of $\Sigma = iGW$, wherein the coupling of the NO σ orbitals into Σ is enhanced by the availablity of NO π orbitals. The energy difference between these sets of orbitals of $\approx$12 eV exceeds the optical band gap, and therefore the energy conservation required by the GW loop can be easily satisfied by electron-hole excitations. We expect that this effect will be general

to nitrates as well as other compounds such as isoelectronic isomers or any compound in which the local orbitals are split in energy, isolating the more-bound valence band states by more than the band gap.

ACKNOWLEDGMENT

The authors wish to thank Eric Shirley for helpful discussions and Jan Weser for assistance with the monochromator calibration.

[1] J. Vinson, T. Jach, W. T. Elam, and J. D. Denlinger, Phys. Rev. B **90**, 205207 (2014).
[2] E. L. Shirley, J. Electron Spectrosc. Relat. Phenom. **110-111**, 305 (2000).
[3] F. Senf, U. Flechsig, F. Eggenstein, W. Gudat, R. Klein, H. Rabus, and G. Ulm, J. Synchrotron Radiat. **5**, 780 (1998).
[4] F. Scholze, B. Beckhoff, G. Brandt, R. Fliegauf, R. Klein, B. Meyer, D. Rost, D. Schmitz, M. Veldkamp, J. Weser *et al.*, Proc. SPIE **4146**, 72 (2000).
[5] R. Unterumsberger, M. Müller, B. Beckhoff, P. Hönicke, B. Pollakowski, and S. Bjeoumikhova, Spectrochim. Acta, Part B **78**, 37 (2012).
[6] M. Müller, B. Beckhoff, R. Fliegauf, and B. Kanngießer, Phys. Rev. A **79**, 032503 (2009).
[7] A. P. Hitchcock and C. E. Brion, J. Electron Spectrosc. Relat. Phenom. **18**, 1 (1980).
[8] J. Vinson, J. J. Rehr, J. J. Kas, and E. L. Shirley, Phys. Rev. B **83**, 115106 (2011).
[9] K. Gilmore, J. Vinson, E. Shirley, D. Prendergast, C. Pemmaraju, J. Kas, F. Vila, and J. Rehr, Comput. Phys. Commun. **197**, 109 (2015).
[10] L. Hedin, Phys. Rev. **139**, A796 (1965).
[11] E. L. Shirley, Phys. Rev. B **58**, 9579 (1998).
[12] E. Kioupakis, D. Steiauf, P. Rinke, K. T. Delaney, and C. G. Van de Walle, Phys. Rev. B **92**, 035207 (2015).
[13] G. Onida, L. Reining, and A. Rubio, Rev. Mod. Phys. **74**, 601 (2002).
[14] R. Haydock, Comput. Phys. Commun. **20**, 11 (1980).
[15] L. X. Benedict and E. L. Shirley, Phys. Rev. B **59**, 5441 (1999).
[16] J. Vinson and J. J. Rehr, Phys. Rev. B **86**, 195135 (2012).
[17] Y. Saad and M. Schultz, SIAM J. Sci. Stat. Comput. **7**, 856 (1986).
[18] E. L. Shirley, Phys. Rev. Lett. **80**, 794 (1998).
[19] Y. Ma, Phys. Rev. B **49**, 5799 (1994).
[20] H. M. Lawler, J. J. Rehr, F. Vila, S. D. Dalosto, E. L. Shirley, and Z. H. Levine, Phys. Rev. B **78**, 205108 (2008).
[21] E. L. Shirley, J. Soininen, G. Zhang, J. Carlisle, T. Callcott, D. Ederer, L. Terminello, and R. Perera, J. Electron Spectrosc. Relat. Phenom. **114-116**, 939 (2001).
[22] T. Minami and K. Nasu, J. Electron Spectrosc. Relat. Phenom. **92**, 231 (1998).
[23] T. Minami, J. Phys. Soc. Jpn. **67**, 3958 (1998).
[24] J. J. Kas, J. J. Rehr, J. A. Soininen, and P. Glatzel, Phys. Rev. B **83**, 235114 (2011).
[25] T. Minami and K. Nasu, Phys. Rev. B **57**, 12084 (1998).
[26] J. Vinson, J. J. Kas, F. D. Vila, J. J. Rehr, and E. L. Shirley, Phys. Rev. B **85**, 045101 (2012).
[27] A. H. England, A. M. Duffin, C. P. Schwartz, J. S. Uejio, D. Prendergast, and R. J. Saykally, Chem. Phys. Lett. **514**, 187 (2011).
[28] T. Mizoguchi, I. Tanaka, S.-P. Gao, and C. J. Pickard, J. Phys. Condens. Matter **21**, 104204 (2009).
[29] F. D. Vila, J. J. Rehr, H. H. Rossner, and H. J. Krappe, Phys. Rev. B **76**, 014301 (2007).
[30] F. Gel'mukhanov, T. Privalov, and H. Ågren, Phys. Rev. B **62**, 13996 (2000).
[31] T. A. Pascal, U. Boesenberg, R. Kostecki, T. J. Richardson, T.-C. Weng, D. Sokaras, D. Nordlund, E. McDermott, A. Moewes, J. Cabana *et al.*, J. Chem. Phys. **140**, 034107 (2014).
[32] F. Vila, J. J. Rehr, J. Kas, R. G. Nuzzo, and A. I. Frenkel, Phys. Rev. B **78**, 121404 (2008).
[33] L. Kong, X. Wu, and R. Car, Phys. Rev. B **86**, 134203 (2012).
[34] C. P. Schwartz, J. S. Uejio, R. J. Saykally, and D. Prendergast, J. Chem. Phys. **130**, 184109 (2009).
[35] P. Giannozzi, S. de Gironcoli, P. Pavone, and S. Baroni, Phys. Rev. B **43**, 7231 (1991).
[36] F. D. Vila, V. E. Lindahl, and J. J. Rehr, Phys. Rev. B **85**, 024303 (2012).
[37] X. Gonze, B. Amadon, P.-M. Anglade, J.-M. Beuken, F. Bottin, P. Boulanger, F. Bruneval, D. Caliste, R. Caracas, M. Côté *et al.*, Comput. Phys. Commun. **180**, 2582 (2009); X. Gonze, G.-M. Rignanese, M. Verstraete, J.-M. Beuken, Y. Pouillon, R. Caracas, F. Jollet, M. Torrent, G. Zerah, M. Mikami *et al.*, Z. Kristallogr. - Crystalline Materials **220**, 558 (2005); X. Gonze, J.-M. Beuken, R. Caracas, F. Detraux, M. Fuchs, G.-M. Rignanese, L. Sindic, M. Verstraete, G. Zerah, F. Jollet *et al.*, Comp. Mat. Sci. **25**, 478 (2002); The ABINIT code is a common project of the Université Catholique de Louvain, Corning Incorporated, and other contributors; http://www.abinit.org.
[38] H. E. Swanson, N. T. Gilfrich, and M. I. Cook, Natl. Bur. Std. Circular 539 **7**, 1 (1957).
[39] J. P. Perdew and Y. Wang, Phys. Rev. B **45**, 13244 (1992).
[40] A. A. Mostofi, J. R. Yates, Y.-S. Lee, I. Souza, D. Vanderbilt, and N. Marzari, Comput. Phys. Commun. **178**, 685 (2008).
[41] W. Humphrey, A. Dalke, and K. Schulten, J. Mol. Graphics **14**, 33 (1996); J. Stone, Master's thesis, Computer Science Department, University of Missouri-Rolla, 1998.
[42] P. Giannozzi, S. Baroni, N. Bonini, M. Calandra, R. Car, C. Cavazzoni, D. Ceresoli, G. L. Chiarotti, M. Cococcioni, I. Dabo *et al.*, J. Phys. Condens. Matter **21**, 395502 (2009).
[43] E. L. Shirley, Phys. Rev. B **54**, 16464 (1996).
[44] D. Prendergast and S. G. Louie, Phys. Rev. B **80**, 235126 (2009).

[45] F. D. Vila, T. Jach, W. T. Elam, J. J. Rehr, and J. D. Denlinger, J. Phys. Chem. A **115**, 3243 (2011).
[46] Calculations were done both with an additional valence electron and for a charged psuedopotenial offset by a uniform background charge, and both methods gave similar results.
[47] F. Gel'mukhanov and H. Ågren, Phys. Rep. **312**, 87 (1999).
[48] L. Weinhardt, E. Ertan, M. Iannuzzi, M. Weigand, O. Fuchs, M. Bar, M. Blum, J. D. Denlinger, W. Yang, E. Umbach *et al.*, Phys. Chem. Chem. Phys. **17**, 27145 (2015).
[49] M. Odelius, H. Ogasawara, D. Nordlund, O. Fuchs, L. Weinhardt, F. Maier, E. Umbach, C. Heske, Y. Zubavichus, M. Grunze *et al.*, Phys. Rev. Lett. **94**, 227401 (2005).